applied sciences

MDPI

Article

Investigation of the Microseismic Response Characteristics of a Bottom Structure's Ground Pressure Activity under the Influence of Faults

Zeng Chen [1,2,*], Da Zhang [1,2], Chang Zuo [3,*], Ping Wang [1,2], Qiang Liu [1,2] and Feng Shi [1,2]

1 BGRIMM Technology Group, Beijing 100160, China
2 National Centre for International Research on Green Metal Mining, Beijing 102628, China
3 School of Energy and Mining Engineering, China University of Mining and Technology Beijing, Beijing 100083, China
* Correspondence: zschenzeng@126.com (Z.C.); sqt2100102050@student.cumtb.edu.cn (C.Z.)

Abstract: To further understand the changing pattern of the bottom structure's ground pressure activity under the influence of faults, predicting the potential occurrence of geological hazards and rock blast problems to reduce the loss of resources is important. A new microseismic monitoring system was established based on the original Pulang copper mine microseismic monitoring system. This paper analyzed the change law of the microseismic events on the fault in the first mining area of the Pulang copper mine, calculated the cumulative apparent volume and energy index changes of the microseismic events near the fault base, and quantitatively analyzed the microseismic event anomalies under the influence of the fault. The results show that rupture of the rock makes the cumulative apparent volume and energy index change significantly, while the timeliness of both makes the cumulative apparent volume predictive of the occurrence of rock fracture and rockburst, and the number of microseismic events corresponds to the intensity of the fault activation, which plays a predictive and guiding role in the subsequent study of fault activation, stability monitoring, and safe production in the mine area of Pulang copper mine.

Keywords: microseismic monitoring; faults; apparent volume; energy density; monitoring and warning

check for updates

Citation: Chen, Z.; Zhang, D.; Zuo, C.; Wang, P.; Liu, Q.; Shi, F. Investigation of the Microseismic Response Characteristics of a Bottom Structure's Ground Pressure Activity under the Influence of Faults. *Appl. Sci.* **2023**, *13*, 3796. https://doi.org/10.3390/app13063796

Academic Editor: Arcady Dyskin

Received: 14 February 2023
Revised: 14 March 2023
Accepted: 14 March 2023
Published: 16 March 2023

1. Introduction

Due to the existence of ground stress and some natural geological formations (folds, faults, etc.), a series of mining disasters such as rock bursts, roofing, sheeting, bottom drums, etc., have been experienced by many countries such as Australia, China, Japan, Germany, Canada, South Africa, etc. [1–7].

In order to predict and prevent this engineering geological problem, many methods have been proposed and applied in laboratory simulations and field experiments, among which microseismic monitoring technology has been widely used as a geophysical method in mining engineering in recent decades by way of locating the fracture breeding and fracture signals during tunneling construction and working face mining [8–14].

In recent years, microseismic monitoring and positioning methods have achieved effective results [15–21]. To eliminate the localization error of the MS/AE monitoring system caused by the wave velocity bias, an MS or AE source localization method without premeasurement of the wave velocity was proposed by Dong [22]. This method not only reduced the localization error caused by the velocity measurement bias but also located the MS/AE source in real time, which made the mine TM method usefully supplemented. A microseismic event localization method based on interferometric imaging and cross-wavelet transform was proposed by Huang [23] to improve the localization accuracy of microseismic event monitoring. As an inevitable geological structure in coal mining

activities, microseismic monitoring is often used to predict and analyze the activation performance due to mining activities, and in this regard, the 14,310 working face of the Dongtan Mine through the NF6 fault was taken as the research object by Chen [24]. The team studied the mechanism of rock explosion induced by the regional surrounding rock activity using relevant mathematical models and explored the microseismic law of the coal mining working face over the fault. Microseismic monitoring technology was used by Liu and his team to monitor the activation process and coal production status of the small faults affected by the excavation activities in real time and track their development direction, and the results showed that excavation activities have a large impact on fault activation [25]. Through similar and numerical simulations, a new parameter (ERW index) was defined for the analysis of such data; based on microseismic analysis, a new rockburst warning model was developed by Zhang [26]. To improve the accuracy of the rockburst identification, a combined AE and statistical approach was proposed by Wang's team to identify the interaction of microcracks within coal and rock, and the method provided a new means of understanding the formation and distribution of cracks in coal rock bodies [27–29]. With the gradual development of microseismic technology, how to accurately and quickly identify problems became the main problem of microseismic monitoring, and the combination with the framework of machine learning has solved this problem solved effectively. The artificial intelligence recognition method was applied by Peng's team to the signal recognition of microseismic monitoring systems in mining areas, and the recognition results were consistent with the actual situation with an accuracy rate of up to 95% or more. In this way, the confusion caused by manual classification of microseismic events and blasts according to the characteristics of waveform signals was solved, the required source parameters were easily obtained, and the accuracy and timeliness of microseismic event and blast identification were ensured [30]. A new method based on deep learning was proposed by Wamriew's team for processing large amounts of DAS data in real/semi-real time. The proposed neural network was trained on synthetic microseismic data contaminated with real environmental noise from field data and validated in engineering practice. This reduced the manual effort of combing the data, thus maintaining the data integrity and leading to more accurate and reproducible results [31].

Because of the hard rock and complex structure at a fault, monitoring is intermittent, and it is difficult to detect ground stress in non-coal mines, so the results of fault-slip rockburst monitoring have been mainly focused on seismic monitoring. In this regard, a mechanical model of the viscous-slip instability of a fault-slip rockburst was established by Hu [32]. Based on revealing the damage characteristics of this instability, the change law of mining-induced stress and the microseismic signal before the occurrence of a fault-slip rockburst was proposed, and a multiparameter integrated early warning method including mining-induced stress and energy was established. The 3D numerical model was used by Sainoki [33] and applied to study the fault behavior of the Copper Cliff Mine in Canada, revealing the importance of distinguishing between seismic and earthquake fault sliding for optimizing underground mine support systems.

However, from the results obtained so far, most of the actual damage characteristics under the influence of faults were based on similar simulations and numerical simulations [34–36], while the actual geological conditions are variable due to the complexity of the rock mass, and the lack of monitoring and analysis of the actual site will make most of the results not universal and applicable to the variable geological structures; so, the study of microseismic response characteristics under the actual site conditions is of significance. After model experiments and characterization studies for rock damage [37–39], this study analyzed the microseismic data at the over fault of the Pulang copper mine, and by introducing the fault model, apparent volume, and energy distribution characteristics, the microseismic response characteristics of the bottom structure under the influence of the fault were analyzed in all aspects and verified in the field. The advantages are the relevance for microseismic monitoring and the timeliness of the way the data are processed, which

can play a guiding role for subsequent stability study and study of the ground pressure activity pattern.

2. Experimental System

2.1. Monitoring Program

The network topology of the integrated monitoring system for the mining process is shown in Figure 1. The specific arrangement is shown in Figure 2. In the center of the first mining area on the surface (the location of 2# slip shaft) and the surrounding area, two hollow monitoring holes were set up; around the center of the first mining area, three TDR monitoring points were arranged through surface drilling, and one monitoring coaxial cable was laid in each TDR monitoring hole; finally, 20 microvibration sensors (18 single-component sensors and 2 three-component sensors) were laid in the N4, N1, S3, and S6 penetration veins of the 3720 mine level downhole. At the same time, four boreholes were constructed around the first mining area through the surface downward, two single-component microseismic sensors were arranged in each borehole, and 12 sets of stress displacement sensors were installed in the S2 penetration vein at the 3720 exit level.

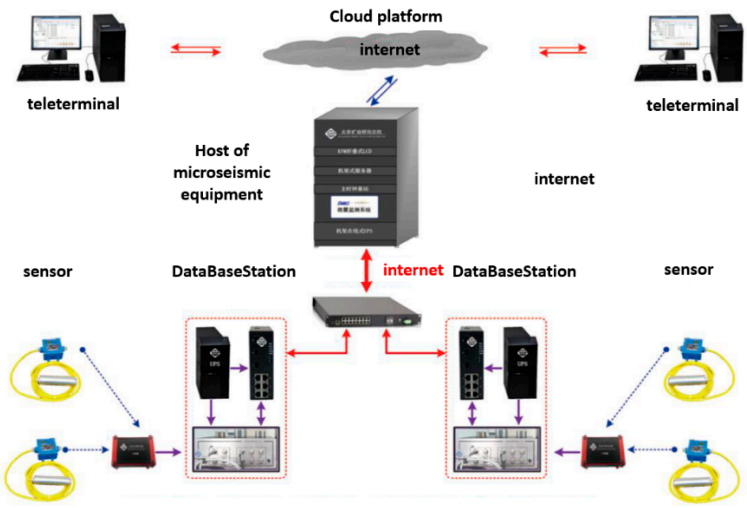

Figure 1. Network topology diagram of the integrated monitoring system for the mining process.

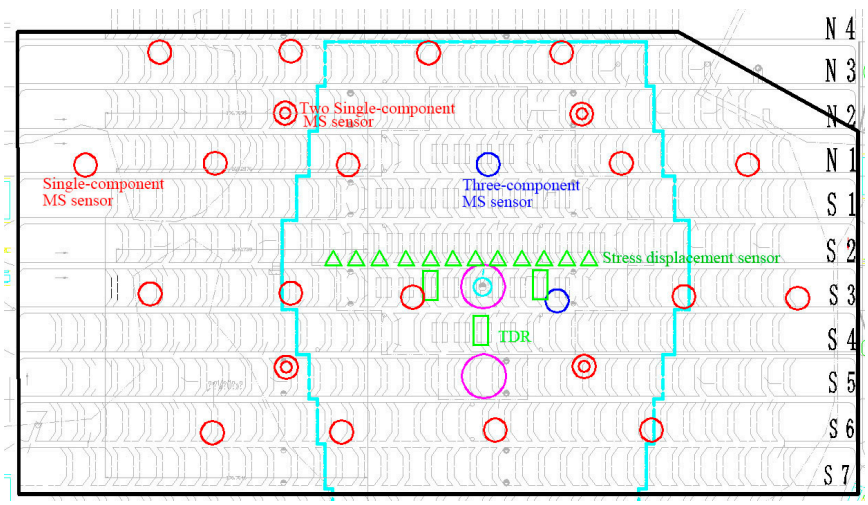

Figure 2. Monitoring point layout. N1–N4, S1–S7 are the label of transverse drift.

The monitoring program was expanded based on the original comprehensive online monitoring system. After the collapse of the surface monitoring area, the monitoring

equipment, such as the empty holes, TDR, and microvibration installed at the surface were removed, and the monitoring focus was shifted to the bottom structure. Based on the preliminary monitoring results and experience, the impact of the revealed fault was fully considered in the later stage, and the bottom structure stability monitoring points were arranged in a targeted manner. Considering the impact of the blasting vibration through the vein, the digital mining substation was installed in the east and west along the outer channel of the vein to reduce the amount of maintenance of the system.

The microseismic monitoring program was designed to move the microseismic digital mining substation on the surface to the 3660 m transport level, and on the basis of the previous monitoring program (there were already four microseismic sensors), to supplement four microseismic sensors and detachable devices to form a spatial three-dimensional envelope with the microseismic sensors arranged at 3720 m to improve the positioning accuracy of the microseismic events. The stress monitoring system was designed to be installed in the pull bottom advance line of the bottom structure at 3720 m, where 24 stress gauges were installed on the key ore pillars, excluding the 12 stress gauges in the pre-S2 penetration vein. The specific monitoring scheme is shown in Figures 3 and 4.

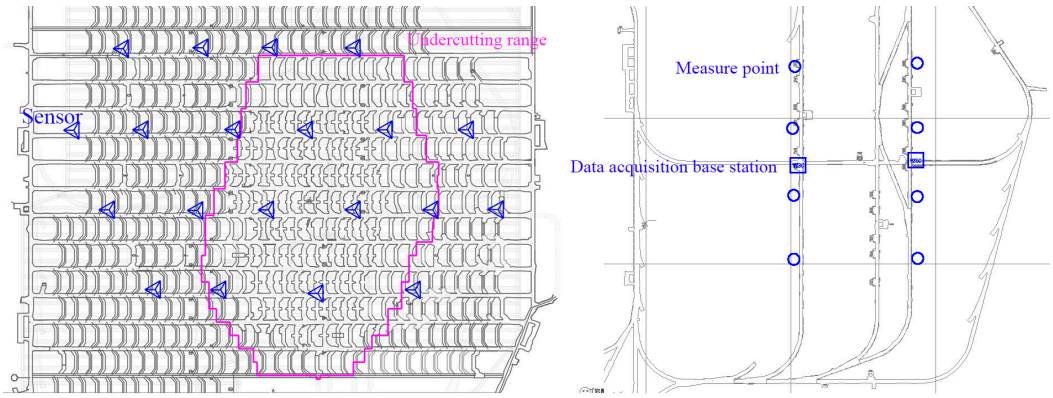

(**a**) (**b**)

Figure 3. Layout of the microseismic monitoring points. (**a**) 3660 m transport level; (**b**) 3720 m exit level.

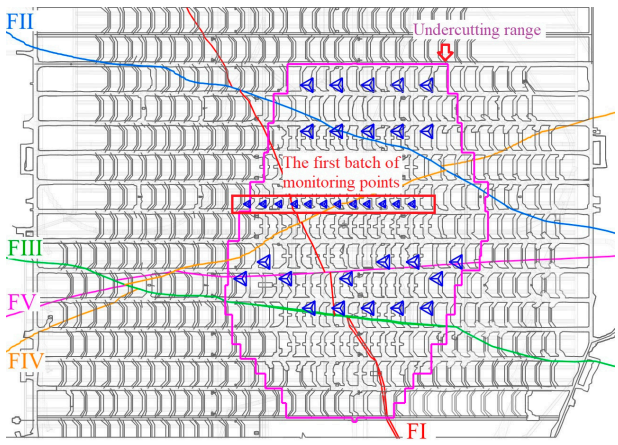

Figure 4. The 3720 m horizontal borehole stress gauge monitoring point layout. FI–FV represent fault.

2.2. Configuration of the System

After the microseismic monitoring system was built, the wave velocity field used to configure the system was the recommended value of the IMS in South Africa. Due to the difference in lithology, the positioning error was large. Therefore, the wave velocity was

finally corrected to V_p = 4700 m/s and V_s = 2700 m/s after several wave velocity corrections through the pull-bottom blasting and poly-mine trough blasting events collected by the microseismic monitoring system.

Under this velocity field model, the positioning accuracy analysis of the two blasts of the poly ore chute on 18 March and 20 March 2017 was conducted; the positioning error of the two blasting events was about 6 m, and the positioning accuracy was high. The blasting event positioning accuracy analysis and results are shown in Table 1.

Table 1. Analysis of blast event positioning accuracy.

Date	Coordinates	Actual Blasting Coordinates/m	Microseismic System Positioning Coordinates/m	Error/m	
				Coordinates	Straight Line
18 March 2017 19:01:04	E	17,597,327.3	17,597,330.8	3.5	5.9
	N	3,103,174.1	3,103,172.3	1.8	
	U	3731.0	3735.5	4.5	
20 March 2017 19:05:55	E	17,597,296.4	17,597,294.9	1.5	6.1
	N	3,103,174.1	3,103,174.0	0.1	
	U	3731.0	3725.1	5.9	

2.3. Monitoring System Error and Sensitivity Calibration

The microseismic monitoring network was calculated according to the three-dimensional spatial arrangement scheme of the microseismic monitoring points, and the positioning error and sensitivity of the 3720 m bottom structure microseismic monitoring system were analyzed, as shown in Figure 5. The analysis of the network showed that the microseismic monitoring system had a positioning error in the first mining area within 10 m, and the microseismic events with a minimum of −2.7 magnitude were monitored with guaranteed accuracy, which met the requirements for monitoring the stability of the substructure.

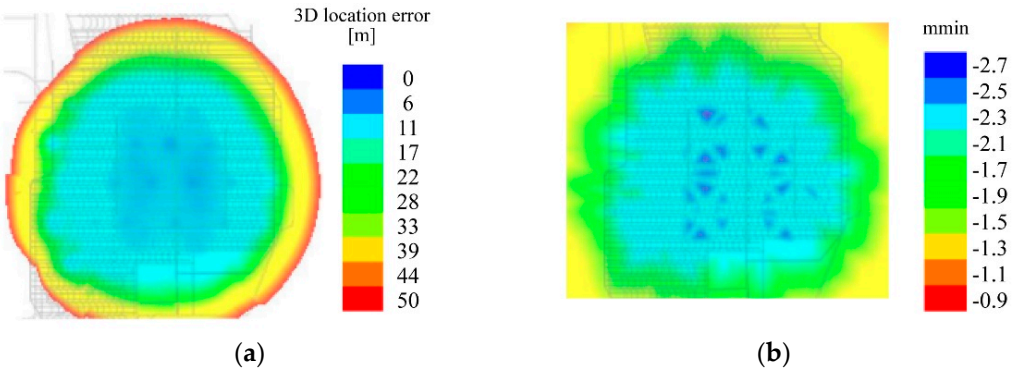

Figure 5. Positioning error analysis and sensitivity analysis of the 3720 m bottom structure microseismic monitoring system. (**a**) Error analysis. (**b**) Sensitivity analysis.

3. Theoretical Foundation

The microseismic signals were received by the microseismic monitoring system, and the rich information, such as the temporal and spatial intensity, contained in each event were obtained after manual processing. By analyzing the changes in the number, density, and concentration of the microfracture, the macroscopic development trend of rocks could be inferred, and the analysis process was based on statistics to convert the rich information of the microseismic events. In this study, we mainly used the cumulative apparent volume and energy index analysis, which were based on the statistical analysis of the microrupture magnitude, microrupture energy, apparent stress, apparent volume, and energy index.

The apparent volume refers to the source volume, which is the volume of the rock in the inelastic deformation zone of the source, and it can be estimated by Equation (1), where $\Delta\varepsilon$ is the incremental body strain in the inelastic zone of the source.

$$V_{\mathrm{A}} = \frac{P}{\varepsilon_{\mathrm{A}}} = \frac{\mu P^2}{E} \tag{1}$$

where μ is the stiffness of the rock (shear modulus). The apparent volume is a scalar quantity, which is closely related to the microseismic body potential and microseismic energy and can be expressed by methods such as the cumulative volume or contour plots.

The energy index EI of a microseismic event is the ratio of the measured radiative microseismic energy E generated by the event to the average microseismic energy $\overline{E}(P)$ of all events in the region, which corresponds to the driving stress of the source at the time of the microseismic event, as shown in Equation (2).

$$EI = \frac{E}{\overline{E}(P)} = \frac{E}{10^{d\log_p + c}} = 10^{-c}\frac{E}{P^d} \tag{2}$$

In Equation (2), C is the correction factor, and the average energy $\overline{E}(P)$ can be obtained from the actual measured average energy in the region and the microseismic body variation potential P in relation to $10^{d\log_p + c}$. When $d = 1$, the average energy is proportional to the apparent stress.

4. Analysis of the Microseismic Event Monitoring Results

4.1. Analysis of the Detection Results of the Number of Microseismic Anomalies over Faults

Figure 6 shows the characteristics of the changes in the number of microseismic events at the five faults over the Pulang copper mine. The microseismic events occurred more frequently from April to August 2018 and from April to July 2019, with the relatively highest number of microseismic events at the five faults on the FIII-2 fault and the lowest number on the FIII-1, among which an abnormal number of microseismic events occurred on 14 June 2019 near the intersection area of the western bottom pushing line and the FI-1, FII-1, and FII-2 faults (as marked by the green dashed line in the figure). To address this abnormal number, the fault model was introduced with the monitoring range as the boundary as shown in Figure 7. In the figure, the yellow is the F1 fault, the red is the F2 fault, the blue is the F3 fault, the purple is the F4 fault, and the green is the F5 fault.

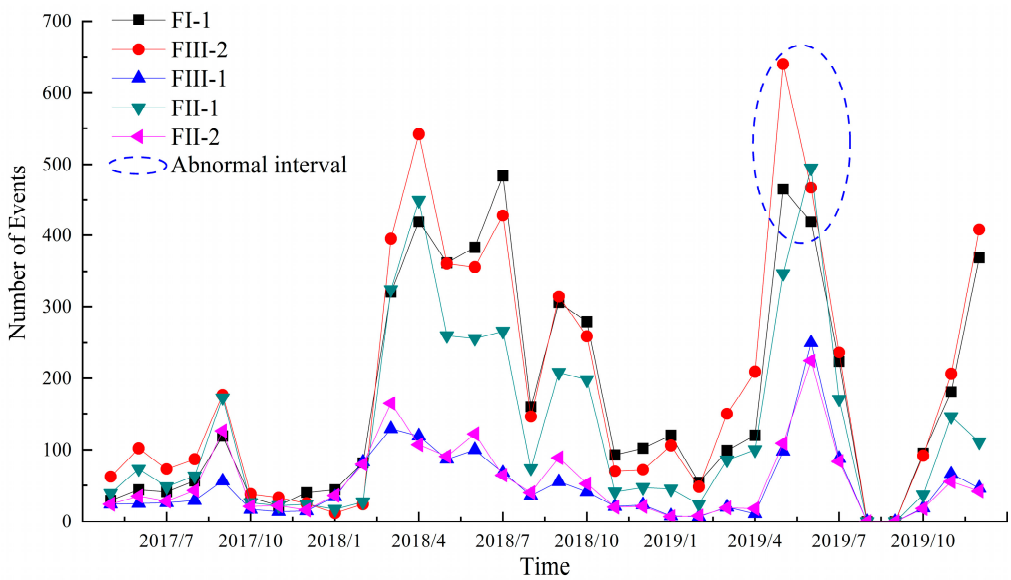

Figure 6. Characteristics of the changes in the number of the microseismic events at the faults.

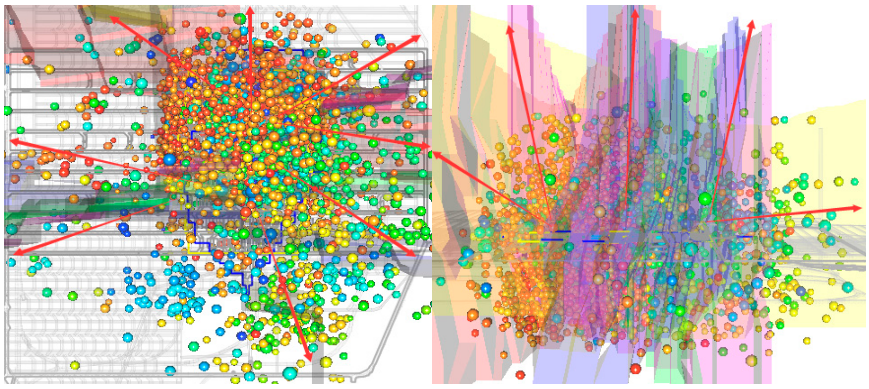

(**a**) (**b**)

Figure 7. Distribution of the microseismic events at the faults. (**a**) Horizontal distribution. (**b**) Vertical distribution. The different colored spheres represent the degree of aggregation of microseismic events near different faults, and the direction of the arrow indicates the development of stress distribution and fault activation due to copper mining.

From Figure 7, it can be seen that microseismic events existed near each fault, among which more microseismic events were generated near the F1, F2, and F4 faults, and the microseismic events were mainly concentrated near the agglomerate groove and pull-bottom advance line, indicating that the rupture events of the rock body caused by the agglomerate groove, pull-bottom, and excavation blasting, the stress redistribution after exiting the mine, and the fault activation showed a certain clustering phenomenon, and gradually developed in all directions along the fault. The microseismic events in the western and northern parts of the first mining area were more concentrated, indicating that the rock rupture in the western and northern parts of the first mining area was more serious, which was consistent with the larger subsidence of the surface 2# chute and its northwestern part. Through the analysis of the fault model, the precursor warning information of the large rupture and destabilization of the rock near the fault was obtained; the pulling-bottom speed and ore output should be controlled in the subsequent production, and the influence of the fault activation on the stability of the rock should be fully considered to strengthen the support measures.

In total, 228 microseismic events were monitored within the green circle during the time period of a number of anomalies at the fault, as shown in Figure 8, in which 213 microseismic events were monitored in the event concentration from 14:00 to 15:00 for about one hour, with the magnitude range −3.6~−2.3. For this microseismic event aggregation phenomenon, a module was established in the region, and its apparent volume and energy analysis were calculated.

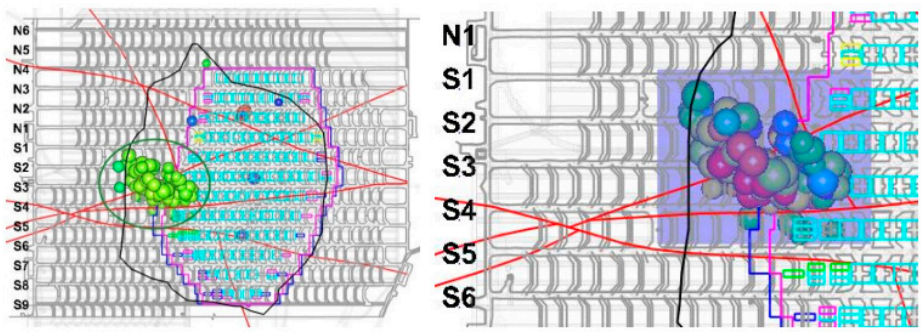

Figure 8. Distribution of the microseismic events at fault. The red lines indicate the distribution of faults. The green circles in the left panel represent the large number of microseismic events collected in a short period of time. For this phenomenon, a module was created in the right figure and its apparent volume and energy analysis were calculated.

The anomalous time interval of the region was intercepted and plotted with the time distribution characteristics of the cumulative apparent volume and energy index as shown in Figure 9. The cumulative apparent volume increased rapidly from 14:00 to 15:00 on that day, while the energy index did not fluctuate, indicating that the rock body in the region produced a microrupture in a short period of time, and no precursor of the rock explosion and large-scale rock collapse was found. The energy index continued to rise around 17:00, indicating that the stress in the region was not released to due to the rupture but continued to accumulate, and might suddenly decrease after accumulating to a certain amount, causing rock bursts and large-scale rock collapse. The cumulative apparent volume was strongly correlated with the occurrence time of the microseismic events, while the change in the energy index required time and energy accumulation. In contrast, the cumulative apparent volume as an observation tool can increase the prediction of the propensity of rock bursts, and after the occurrence of the abnormal monitoring, the surface subsidence monitoring of the northwest area of the first mining area on the same day issued a subsidence alarm at 00:26. Therefore, we infer that this microseismic event aggregation phenomenon for the west side of the mining area subsidence led to fault activation, which in turn caused a large number of microrupture phenomena in the regional rock body for a short period of time.

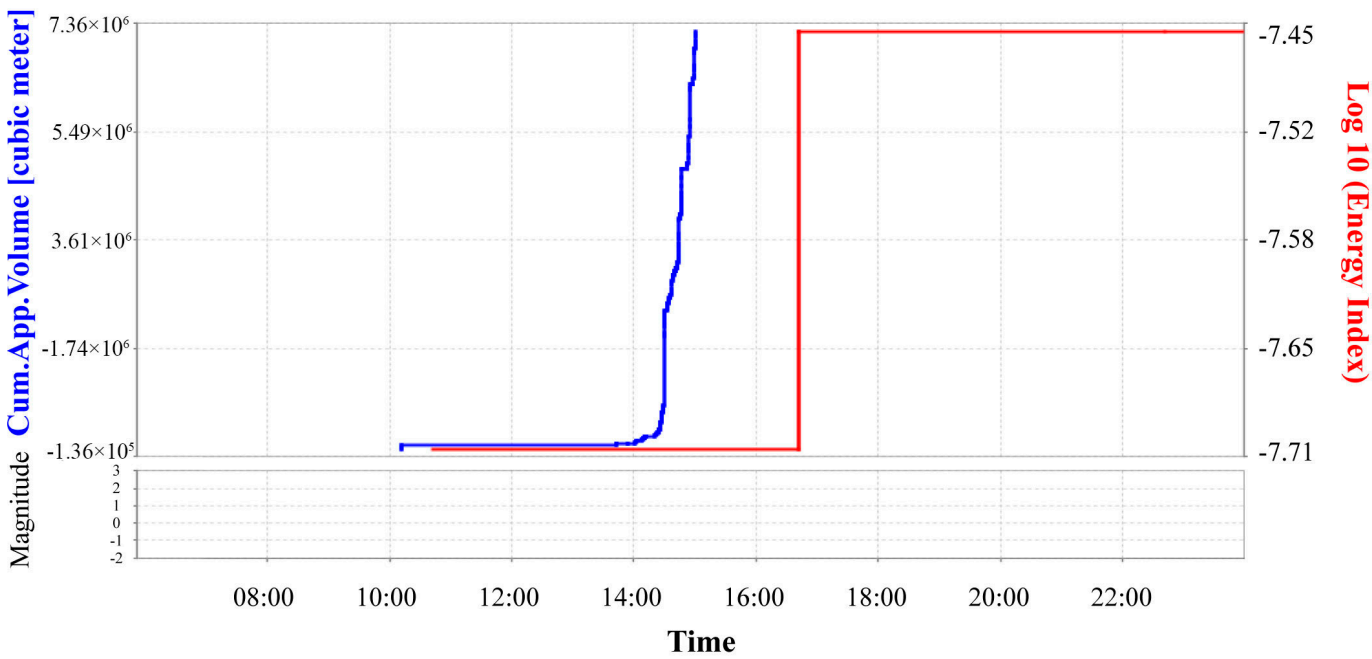

Figure 9. Analysis module of the cumulative apparent volume and energy index time distribution characteristics.

4.2. Verification of the Monitoring Results and Site Conditions

The microseismic anomaly area was surveyed to verify the accuracy of the microseismic monitoring and apparent volume energy prediction, and the survey results were consistent with the actual monitoring and predicted results based on the investigation of the field conditions in the microseismic event anomaly area at the 3736 m level. These findings suggest that the microseismic event monitoring of the over fault and the apparent volume and energy indices are reliable for the prediction of rockburst and large-scale ruptures that may be caused by fault activation. Figure 10 shows the channel fragmentation and deformation of the corresponding area at the 3736 m level on that day.

Figure 10. Roadway crushing and deformation in the corresponding area at the 3736 m level. The red lines depict the fissures due to ground pressure activity.

5. Discussion

Geological structures, especially faults, are very important for the stability control of the roadway, and faults are often seen in mine production. The fault dip distribution in the Pulang copper mine is generally steep, about 60° to 85°, and the thickness is between 0.1 m and 2 m. During the construction of the bottom structure out of the mine through the vein, several roadways inevitably pass directly through the fault. Therefore, the control and monitoring of the faults is of high significance for the safety of the mining activities, and some studies have previously been conducted to investigate the activation properties of faults. Three-dimensional numerical simulations were used by Jiang [40] to study the stress evolution characteristics and the activation law of mining reverse faults under hard and thick layers, to establish a fault model and to derive the stress evolution characteristics of over-reverse faults by mining activities. To investigate the influencing factors and critical water pressure leading to the rupture of hydraulic conductivity faults, a simplified fracture mechanics model was used by Chen [41] to study the sudden water accidents caused by underground hidden faults. Although these approaches achieved effective results, they were only at the model level for fault activation, and there was no real-time monitoring of the suddenness and variability of the disasters caused by fault activation. With the application of microseismic technology in coal mining, microseismic monitoring techniques were used by Zhu and Guo [42,43] and others to achieve real-time monitoring of the activation performance of faults; however, the monitoring data were less processed; so, their monitoring was not an early warning system.

From the results of the above study and analysis, it can be seen that the distribution pattern of the microseismic events and the distribution of the apparent volume and energy density with time were predictive for the anomalous results due to fault activation and also provided a basis for the researchers to study the microseismic response studies at the faults; the predictions were consistent with the actual results. The mine activity led to the activation of faults, which in turn led to an increase in the number of microseisms, and as the apparent volume density increased, the the apparent bulk density increased, the energy density continued to accumulate, and the risk factor gradually increased, resulting in tunnel crushing and deformation. When the energy density index suddenly becomes small, mining disasters such as rockbursts and massive rock rupture can occur, and the difference in the timing of the apparent bulk density and energy index makes it possible to make predictions by calculating the bulk density before the sudden changes in energy density, which greatly improves the predictability of rock bursts and coal mine production, safety. The real-time monitoring of the Pulang copper mine is more relevant and timely than the monitoring of ordinary fault models, and this is more statistically significant, predictive, and instructive for the way ordinary monitoring data can be processed.

6. Conclusions

In this research, the monitoring system was improved, the results of the microseismic events were analyzed, and the data were processed. The following three conclusions were obtained from the data from the real-time monitoring using the cumulative apparent volume and energy index algorithms.

(1) On the basis of the original monitoring system, a monitoring system suitable for the bottom stability of the first mining section of the Pulang copper mine was established, and the design of the bottom structural stability monitoring scheme and system construction were completed on the premise of ensuring the accuracy and reliability of monitoring data and reducing the maintenance of the system, which met the testing requirements after the error and sensitivity calibration and debugging.

(2) Using the cumulative apparent volume and energy indices to visualize the propensity for rockbursts, the rise in the cumulative apparent volume leads to an increase in the number of rock ruptures, while the rise in energy index indicates a continuous accumulation of energy density with a tendency to rockburst; the timeliness of both makes the cumulative apparent volume predictive of rock rupture and rockburst occurrence.

(3) The test results are timely and standardized compared with conventional monitoring and physical simulation. In addition, the test results guide the prediction of rockburst propensity, the analysis of fault activation mechanisms, and the safety of over-fault coal mine operations.

Author Contributions: Conceptualization, Z.C. and C.Z.; data curation, D.Z., P.W. and Q.L.; formal analysis, F.S.; project administration, D.Z.; resources, Z.C., D.Z. and P.W.; visualization, Z.C., Q.L. and F.S.; writing—original draft, Z.C. and C.Z. All authors have read and agreed to the published version of the manuscript.

Funding: This research was funded by the Youth Science and Technology Innovation Fund, BGRIMM Technology Group (Grant No. 04-2228), and the National Key Research and Development Program of China (Grant No. 2017YFC0602904).

Institutional Review Board Statement: Not applicable.

Informed Consent Statement: Not applicable.

Data Availability Statement: The data used to support the findings of this study are available from the corresponding author upon request.

Acknowledgments: We thank Cong Cao, Baokun Zhou, and Changfeng Li for improving the manuscript.

Conflicts of Interest: The authors declare no conflict of interest.

References

1. Abdul-Wahed, M.K.; Al Heib, M.; Senfaute, G. Mining-induced seismicity: Seismic measurement using multiplet approach and numerical modelling. *Int. J. Coal Geol.* **2006**, *66*, 137–147. [CrossRef]
2. Driad-Lebeau, L.; Lahaie, F.; Al Heib, M.; Josien, J.; Bigarré, P.; Noirel, J.F. Seismic and geotechnical investigations following a rockburst in a complex French mining district. *Int. J. Coal Geol.* **2005**, *64*, 66–78. [CrossRef]
3. Lasocki, S.; Orlecka-Sikora, B. Seismic hazard assessment under complex source size distribution of mining-induced seismicity. *Tectono-Phys.* **2008**, *456*, 28–37. [CrossRef]
4. Leśniak, A.; Isakow, Z. Space–time clustering of seismic events and hazard assessment in the Zabrze–Bielszowice coal mine, Poland. *Int. J. Rock Mech. Min. Sci.* **2009**, *46*, 918–928. [CrossRef]
5. Mansurov, V.A. Prediction of rockbursts by analysis of induced seismicity data. *Int. J. Rock Mech. Min. Sci.* **2001**, *38*, 893–901. [CrossRef]
6. Šílený, J.; Milev, A. Source mechanism of mining induced seismic events—Resolution of double couple and non double couple models. *Tectonophysics* **2008**, *456*, 3–15. [CrossRef]
7. Hudyma, M.; Potvin, Y.H. An engineering approach to seismic risk management in hardrock mines. *Rock Mech. Rock Eng.* **2010**, *43*, 891–906. [CrossRef]
8. Dong, L.J.; Wesseloo, J.; Potvin, Y.; Li, X.B. Discrimination of mine seismic events and blasts using the Fisher classifier, naive Bayesian classifier and logistic regression. *Rock Mech. Rock Eng.* **2016**, *49*, 183–211. [CrossRef]

9. Dong, L.J.; Wesseloo, J.; Potvin, Y.; Li, X.B. Discriminant models of blasts and seismic events in mine seismology. *Int. J. Rock Mech. Min. Sci.* **2016**, *86*, 282–291. [CrossRef]
10. Lu, C.P.; Liu, Y.; Wang, H.Y.; Liu, P.F. Microseismic signals of double-layer hard and thick igneous strata separation and fracturing. *Int. J. Coal Geol.* **2016**, *160–161*, 28–41. [CrossRef]
11. Dong, L.; Li, X.; Xie, G. Nonlinear methodologies for identifying seismic event and nuclear explosion using random forest, support vector machine, and naive Bayes classification. *Abstr. Appl. Anal.* **2014**, *2014*, 459137. [CrossRef]
12. Song, D.; Wang, E.; Li, Z.; Qiu, L.; Xu, Z. EMR: An effective method for monitoring and warning of rock burst hazard. *Geomech. Eng.* **2017**, *12*, 53–69. [CrossRef]
13. Hirata, A.; Kameoka, Y.; Hirano, T. Safety management based on detection of possible rock bursts by AE monitoring during tunnel excavation. *Rock Mech. Rock Eng.* **2007**, *40*, 563–576. [CrossRef]
14. He, J.; Dou, L.; Gong, S.; Li, J.; Ma, Z. Rock burst assessment and prediction by dynamic and static stress analysis based on micro-seismic monitoring. *Int. J. Rock Mech. Min. Sci.* **2017**, *93*, 46–53. [CrossRef]
15. Zhao, T.B.; Guo, W.Y.; Yu, F.H.; Tan, Y.L.; Huang, B.; Hu, S.C. Numerical investigation of influences of drilling arrangements on the mechanical behavior and energy evolution of coal models. *Adv. Civ. Eng.* **2018**, *2018*, 3817397. [CrossRef]
16. Qiu, L.; Song, D.; Li, Z.; Liu, B.; Liu, J. Research on AE and EMR response law of the driving face passing through the fault. *Saf. Sci.* **2019**, *117*, 184–193. [CrossRef]
17. Zhang, Z.Z.; Gao, F.; Shang, X.J. Rock burst proneness prediction by acoustic emission test during rock deformation. *J. Cent. South Univ.* **2014**, *21*, 373–380. [CrossRef]
18. Wang, E.; He, X.; Wei, J.; Nie, B.; Song, D. Electromagnetic emission graded warning model and its applications against coal rock dynamic collapses. *Int. J. Rock Mech. Min. Sci.* **2011**, *48*, 556–564. [CrossRef]
19. He, X.; Chen, W.; Nie, B.; Mitri, H. Electromagnetic emission theory and its application to dynamic phenomena in coal-rock. *Int. J. Rock Mech. Min. Sci.* **2011**, *48*, 1352–1358. [CrossRef]
20. He, M.C.; Miao, J.L.; Feng, J.L. Rock burst process of limestone and its acoustic emission characteristics under true-triaxial unloading conditions. *Int. J. Rock Mech. Min. Sci.* **2010**, *47*, 286–298. [CrossRef]
21. Cai, W.; Dou, L.; Zhang, M.; Cao, W.; Shi, J.Q.; Feng, L. A fuzzy comprehensive evaluation methodology for rock burst forecasting using microseismic monitoring. *Tunn. Undergr. Space Technol.* **2018**, *80*, 232–245. [CrossRef]
22. Dong, L.; Sun, D.; Li, X.; Du, K. Theoretical and Experimental Studies of Localization Methodology for AE and Microseismic Sources Without Pre-Measured Wave Velocity in Mines. *IEEE Access* **2017**, *5*, 16818–16828. [CrossRef]
23. Huang, L.Q.; Hao, H.; Li, X.B.; Li, J. Source identification of microseismic events in underground mines with interferometric imaging and cross wavelet transform. *Tunn. Undergr. Space Technol.* **2018**, *71*, 318–328. [CrossRef]
24. Chen, X.H.; Li, W.Q.; Yan, X.Y. Analysis on rock burst danger when fully-mechanized caving coal face passed fault with deep mining. *Saf. Sci.* **2012**, *50*, 645–648. [CrossRef]
25. Liu, C.; Li, S.G.; Cheng, C.; Xue, J.H. Activation characteristics analysis on concealed fault in the excavating coal roadway based on microseismic monitoring technique. *Int. J. Min. Sci. Technol.* **2017**, *27*, 883–887. [CrossRef]
26. Zhang, C.; Jin, G.H.; Liu, C.; Li, S.G. Prediction of rockbursts in a typical island working face of a coal mine through microseismic monitoring technology. *Tunn. Undergr. Space Technol.* **2021**, *113*, 103972. [CrossRef]
27. Wang, C.L.; Liu, Y.B.; Hou, X.L.; Elmo, D. Investigation of the spatial distribution pattern of 3D microcracks in single-cracked breakage. *Int. J. Rock Mech. Min. Sci.* **2022**, *154*, 105126. [CrossRef]
28. Wang, C.L.; Zhou, B.K.; Li, C.F. Experimental investigation on the spatio-temporal-energy evolution pattern of limestone fracture using acoustic emission monitoring. *J. Appl. Geophys.* **2022**, *206*, 104787. [CrossRef]
29. Wang, C.L.; Hou, X.L.; Liu, Y.B. Three-Dimensional Crack Recognition by Unsupervised Machine Learning. *Rock Mech Rock Eng.* **2021**, *54*, 893–903. [CrossRef]
30. Peng, K.; Tang, Z.; Dong, L.; Sun, D. Machine Learning Based Identification of Microseismic Signals Using Characteristic Parameters. *Sensors* **2021**, *21*, 6967. [CrossRef]
31. Wamriew, D.; Pevzner, R.; Maltsev, E.; Pissarenko, D. Deep Neural Networks for Detection and Location of Microseismic Events and Velocity Model Inversion from Microseismic Data Acquired by Distributed Acoustic Sensing Array. *Sensors* **2021**, *21*, 6627. [CrossRef]
32. Hu, S.C.; Tan, Y.L.; Ning, J.G. Multiparameter Monitoring and Prevention of Fault-Slip Rock Burst. *Shock Vib.* **2017**, *2017*, 7580109. [CrossRef]
33. Sainoki, A.; Mitri, H.S.; Chinnasane, D. Characterization of Aseismic Fault-Slip in a Deep Hard Rock Mine Through Numerical Modelling: Case Study. *Rock Mech. Rock Eng.* **2017**, *50*, 2709–2729. [CrossRef]
34. Qu, X.C.; Jiang, F.X.; Yu, Z.X.; Ju, H.Y. Rockburst monitoring and precaution technology based on equivalent drilling research and its applications. *Chin. J. Rock Mech. Eng.* **2011**, *30*, 2346–2351.
35. Liu, J.H.; Di, M.H.; Guo, X.S.; Jiang, F.X.; Sun, G.J.; Zhang, Z.W. Theory of coal burst monitoring using technology of vibration field combined with stress field and its application. *J. China Coal Soc.* **2014**, *39*, 353–363. [CrossRef]
36. Cao, A.; Dou, L.; Cai, W.; Gong, S. Case study of seismic hazard assessment in underground coal mining using passive tomography. *Int. J. Rock Mech. Min. Sci.* **2015**, *78*, 1–9. [CrossRef]
37. Wang, C.L.; Chen, Z.; Liao, Z.F.; Hou, X.L. Experimental investigation on predicting precursory changes in entropy for the dominant frequency of rockburst. *J. Cent. South Univ.* **2020**, *21*, 2834–2848. [CrossRef]

38. Wang, C.L.; Li, C.F.; Chen, Z.; Liao, Z.F. Experimental investigation on multi-parameter classification predicting degradation model for rock failure using Bayesian method. *Geomech. Eng.* **2020**, *20*, 113–120. [CrossRef]
39. Wang, C.L.; Chuai, X.S.; Hou, X.L.; Chen, Z. Experimental investigation of predicting points using Tangent damage factor for limestone failure. *J. Appl. Geophy.* **2020**, *178*, 104056. [CrossRef]
40. Jiang, J.Q.; Wu, Q.L. Characteristic of mining stress evolution and activation of the reverse fault below the hard-thick strata. *J. China Coal Soc.* **2015**, *40*, 267–277. [CrossRef]
41. Chen, Z.H.; Hu, Z.P.; Li, H.; Chen, Q.F. Fracture mechanical model and criteria of insidious fault water inrush in coal mines. *J. China Univ. Min. Technol.* **2011**, *40*, 673–677.
42. Zhu, S.T.; Jiang, F.X. Fault activation of fully mechanized caving face in extra-thick coal seam of deep shaft. *Chin. J. Rock Mech. Eng.* **2016**, *35*, 50–58. [CrossRef]
43. Guo, X.Q.; Dou, L.M. Research on the Microseismic activity of fault reaction induced by coal mining. *Saf. Coal Mines* **2011**, *42*, 26–30. [CrossRef]